

Supplementary Information

Exfoliation of Covalent Organic Frameworks into Few-Layer Redox-Active Nanosheets as Cathode Materials for Lithium-Ion Batteries

Shan Wang, Qianyou Wang, Pengpeng Shao, Yuzhen Han, Xing Gao, Li Ma, Shuai Yuan, Xiaojie Ma, Junwen Zhou, Xiao Feng,* Bo Wang*

- 1. Materials and methods**
- 2. Synthetic procedures**
- 3. Electrochemical Tests**
- 4. Supplementary Figures**

1. Materials and methods

All chemicals and solvents were purchased from commercial suppliers including Energy Chemical Co., Ltd., J&K Chemical Co., Ltd., TCI (Shanghai) Development Co., Ltd. and Beijing Chemical Reagent Company, and used without further purification. Powder X-ray diffraction (PXRD) patterns of the samples were measured with a Cu-K α X-ray radiation source ($\lambda = 0.154056$ nm) incident radiation by a Rigaku MiniFLEX 600 instrument operating at 40 kV and 50 mA current. The Fourier transform infrared attenuated total reflection (FTIR-ATR) spectra were recorded in the range 400-4000 cm⁻¹ on Bruker ALPHA spectrometer. The measurement of Brunauer-Emmett-Teller (BET) surface area and pore size were performed at 77 K on a Quantachrome Instrument ASiQMVH002-5 after pretreatment (samples were degassed at 180 °C for 12 h). Elemental analyses including C, H, N were measured by VARIO EL-III Elemental Analyzer. ¹H NMR spectra were recorded on a Bruker ARX-400 spectrometer. The solid-state ¹³C magic angle spinning (MAS) nuclear magnetic resonance (NMR) experiments were performed on Agilent DD2 NMR 400MHz NMR Spectrometer with one NMR probe. Thermogravimetric analyses (TGA) were carried out on a TG50 analyzer (Mettler-Toledo) under N₂ atmosphere at a heating rate of 10 °C min⁻¹ within a temperature range of 20-600 °C. Prior to the transmission electron microscopy (TEM), field-emission scanning electron microscopy (FE-SEM) and atomic force microscopy (AFM) characterization, the methanol suspension of exfoliated COF nanosheets was dropped onto the holey carbon-coated carbon support copper grids, Si/SiO₂ and piranha-cleaned Si/SiO₂, respectively, and then naturally dried. TEM images were acquired on JEM-2010 with an electron acceleration energy of 200 kV. FE-SEM images were acquired from a JEOL model S-4800 scanning electron microscope. AFM (Cypher, Asylum Research) was used to characterize the exfoliation COF in tapping mode in air.

2. Synthetic procedures

2-1. Synthesis of 1,3,5-tris(4-formylphenyl)benzene (TFP)

1,3,5-tris(4-formylphenyl)benzene (TFP) was synthesized according to a reported procedure with slight modification.^[1] Under a nitrogen atmosphere, hexamethylenetetramine (15.098 g, 108 mmol) and m-trihydroxybenzene (6.014 g, 49 mmol) were added to a solution of 90 mL CF₃COOH in a 500 mL three-necked bottle at 25 °C. The mixture was heated at 70 °C and stirred for 1.5 hours. Then 150 mL of 3 M HCl was added to the reaction solution and reacted for another 2 hours. After cooling to room temperature, the reaction mixture was filtered and extracted with ca. 200 mL dichloromethane. The filtrate was concentrated on a rotary evaporator. The crude residue was purified by washing with hot ethanol to give pure TFP as a yellow solid, 1.24 g (12% yield). ¹H NMR (400 MHz, CDCl₃): δ 14.12 (s, 3H, OH), 10.16 (s, 3H, CHO) ppm.

2-2. Synthesis of DAAQ-TFP-COF

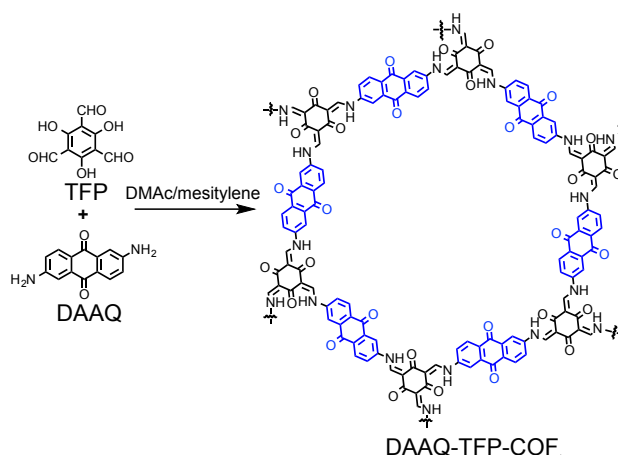


Figure S1. Synthesis route for DAAQ-TFP-COF.

DAAQ-TFP-COF was synthesized according to a reported procedure with slight modification.^[2] A 10 mL Pyrex tube was charged with 1,3,5-tris(4-formylphenyl)benzene (TFP) (20 mg, 0.095 mmol), 2,6-diaminoanthraquinone (DAAQ) (34 mg, 0.142 mmol), 0.9 mL DMAc and 0.3 mL mesitylene. The resulting suspension was sonicated for 30 seconds at room temperature, and then added 50 µL portion of 6 M acetic acid. The tube was freeze-pump-thaw 3 cycles and sealed off and heated at 120 °C for 3 days. The resulting dark-red powder was collected by filtration and washed with DMF (10 × 20

mL) and acetone (3×20 mL), then dried at $180\text{ }^{\circ}\text{C}$ under vacuum for 24 hours to give a deep red colored powder in 73% (36 mg) isolated yield.

2-4. Synthesis of DABQ-TFP-COF

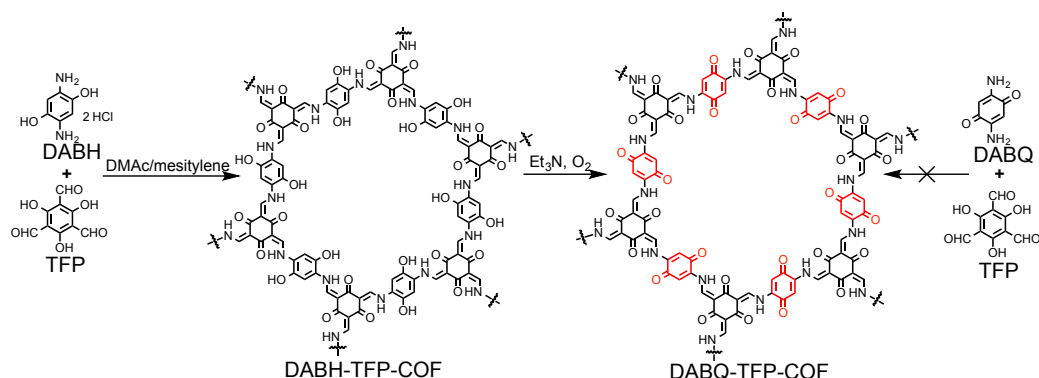


Figure S2. Synthesis route for DABQ-TFP COF.

A 10 mL Pyrex tube was charged with 1,3,5-tris(4-formylphenyl)benzene (TFP) (20 mg, 0.095 mmol), 2,5-diamino-1,4-dihydroxybenzene dihydrochloride (DABH) (30 mg, 0.142 mmol), 0.6 mL DMAc and 0.6 mL mesitylene. The resulting suspension was sonicated for 30 seconds at room temperature, and then added 50 μL portion of 6 M acetic acid. The tube was freeze-pump-thaw 3 cycles and sealed off and heated at $120\text{ }^{\circ}\text{C}$ for 3 days. The resulting dark powder was collected by filtration and washed with DMF (3×20 mL) and acetone (3×20 mL), then dried at $120\text{ }^{\circ}\text{C}$ under vacuum for 24 hours to give DABH-TFP-COF in 87% isolated yield (30 mg, black powder).

50 mg DABH-TFP-COF was dissolved in 5 mL triethylamine, the suspension was stirred in air at room temperature overnight, then the precipitate was filtered off, washed with THF, acetone, and finally with methanol. Further purification of the materials was carried out by Soxhlet extraction in THF for 12 h. After drying under vacuum, the reaction afforded DABQ-TFP-COF in 80% isolated yield (40 mg, black powder).

2-5. Synthesis of TEMPO-COF

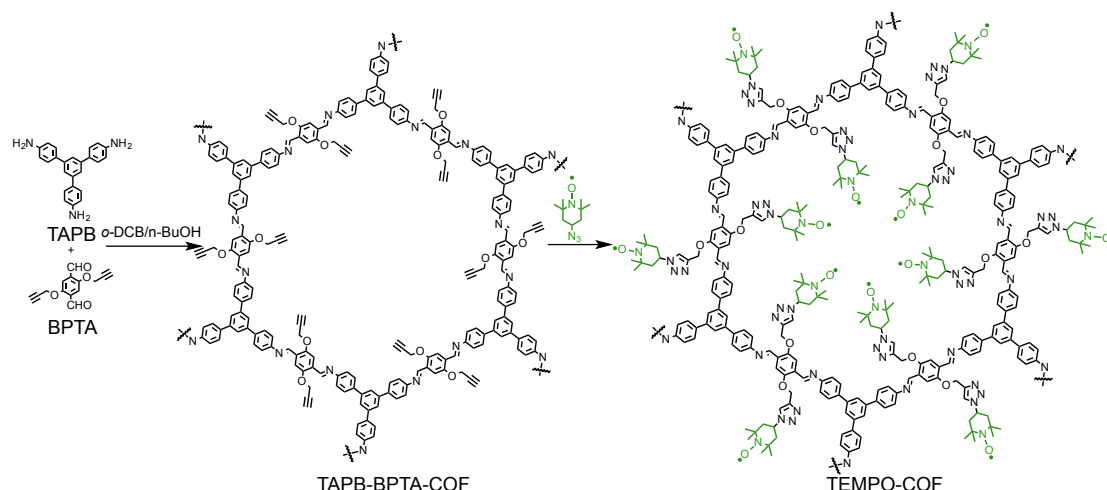


Figure S3. Synthesis route for TEMPO-COF.

2,5-Bis(2-propynyloxy)terephthalaldehyde (BPTA) and 4-azido-2,2,6,6-tetramethylpiperidine 1-oxyl radical were synthesized according to the reported methods.^[3-5]

A 10 mL Pyrex tube was charged with 1,3,5-tri-(4-aminophenyl)benzene (TAPB) (28.1 mg, 0.081 mmol), 2,5-bis(2-propynyloxy)terephthalaldehyde (BPTA) (29 mg, 0.12 mmol), 1 mL *o*-DCB and 1 mL BuOH. The resulting suspension was sonicated for 30 seconds at room temperature, and then added 100 μ L portion of 6 M acetic acid. The tube was freeze-pump-thaw 3 cycles and sealed off and heated at 120 $^{\circ}$ C for 3 days. The resulting yellow powder was collected by filtration and washed with THF (3 \times 20 mL), then dried at 120 $^{\circ}$ C under vacuum for 24 hours to give TAPB-BPTA-COF in 73% isolated yield (36 mg, yellow-green powder).

4-Azido-2,2,6,6-tetramethylpiperidine 1-oxyl radical (60 mg, 0.304 mmol) was added to a THF/water (3 mL/0.5 mL) mixture of TAPB-BPTA-COF (50 mg, 0.195 mol) in the presence of CuI (5 mg) and N,N-diisopropylethylamine (50 μ L) in a 10 mL Pyrex tube. The tube was degassed via three freeze-pump-thaw cycles and sealed off, and the mixture was reacted at room temperature for 24 h. The precipitate was collected via centrifugation, washed five times with THF and acetonitrile, and dried at room temperature under vacuum to produce TEMPO-COF in 80% isolated yield (80 mg, yellow-green powder).

2-6. Synthesis of DAAQ-ECOF, DABQ-ECOF and TEMPO-ECOF

DAAQ-ECOF was prepared by ball-milling method to exfoliate the bulk COFs. In a typical experiment, 150 mg of bulk DAAQ-TFP-COFs were placed in a milling

pot with six steel ball ($\Phi = 3$ mm), and then the mixture was balling at 50 Hz (Jingxin, Tissuelyser-24) for 0.5 h and the delaminated nanosheets were collected for Li ion electrode. In the controlled experiments, the frequencies and ball-milling times were set up at 25 Hz/0.5 h and 60 Hz/2 h for the preparation of DAAQ-ECOF-25Hz and DAAQ-ECOF-60Hz, respectively.

DABQ-ECOF and TEMPO-ECOF were prepared by the same procedures.

3. Electrochemical Tests

Electrochemical measurements were performed using CR2032 coin type cells. The active materials, including DAAQ-TFP-COF, DAAQ-ECOF, DAAQ, DABQ-TFP-COF, DABQ-ECOF, TEMP-COF and TEMPO-ECOF powder, were mixed with conductive carbon black (Super P), polyvinylidene fluoride binder (PVDF) solution (PVDF in *N*-methyl-2-pyrrolidinone (NMP)) with a 6:3:1 weight ratio by using a high-energy ball-milling mixer (50 Hz, 30 min). Then the cathodes were prepared by spreading the slurry on an alumina plate using a coater. After drying in vacuum at 120 °C overnight to remove NMP, the cathode was cut into a round shape with a diameter of 12 mm. The mass loading density of the active materials is uniform and about 0.45 mg cm⁻². The cells were thus fabricated from the cathode, a Celgard 2400 membrane separator, a lithium plate anode and LiTFSI electrolyte (1M) in tetraethylene glycol dimethyl ether (TEGDME). All cells were assembled in an argon-filled glove box. The discharge and charge measurements were carried out on an Land instruments CT2001A testing system in the potential range of 1.5 to 4 V (vs. Li⁺/Li) for DAAQ-TFP-COF, DAAQ-ECOF, DAAQ, DABQ-TFP-COF and DABQ-ECOF; 2 to 4.2 V (vs. Li⁺/Li) for TEMPO-COF and TEMPO-ECOF.

Cyclic voltammetry (CV) and electrochemical impedance spectroscopy (EIS) measurements were both conducted on a CHI 760E electrochemical workstation (Shanghai Putian) using the coin cells. The cutoff voltage of CV test was 1.5-3.5V and different scan rates (1, 2, 3 and 4 mV s⁻¹) were applied. For EIS tests, the voltage amplitude was 10 mV and the frequency range was 100000 Hz–0.01 Hz. All the electrochemical tests were performed at room temperature.

The Nyquist plot for the DAAQ-ECOF cell shows the decrease in the size of the semicircle at high and middle frequency range, comparing to the cell with DAAQ, DAAQ-TFP-COF cathode (Figure S15). It reveals that DAAQ-ECOF exhibits faster charge-transfer kinetics and electric responses with lower resistance in a circuit.^[6-7]

The significant decrease of Warburg impedance in DAAQ-ECOF (Table S2) further confirms the reduction of the diffusion impact on the battery performance for DAAQ-ECOF.

Li-ion diffusion coefficients were obtained by electrochemical impedance spectroscopy (EIS)^[8-10] and derived from Eq. (1):

$$D = 0.5 \left(\frac{RT}{AF^2 \sigma C} \right)^2 \quad (1)$$

where R is the gas constant ($8.314 \text{ J mol}^{-1} \text{ K}^{-1}$), T is the temperature (298.5 K), A is the area of the electrode surface (1.14 cm^2), F is the Faraday's constant ($9.65 \times 10^4 \text{ C mol}^{-1}$), C is the molar concentration of Li^+ , and σ is the Warburg coefficient.

The Warburg coefficient σ can be obtained from Eq. (2):

$$Z_{\text{re}} = R_e + R_{\text{ct}} + \sigma \omega^{-0.5} \quad (2)$$

Where σ is the slope for the plot of Z_{re} vs. the reciprocal root square of the lower angular frequencies ($\omega^{-0.5}$). The obtained σ for DAAQ-TFP-COF and DAAQ-ECOF are 33.1 and 19.8, respectively (Figure S19). As a consequence, DAAQ-ECOF gives a D_{Li^+} of $6.94 \times 10^{-11} \text{ cm}^2 \text{ s}^{-1}$, which is almost three times that of DAAQ-TFP-COF ($2.48 \times 10^{-11} \text{ cm}^2 \text{ s}^{-1}$) and is much higher than those of many commercial electrode materials (Table S3). The high Li-ion diffusion coefficients for DAAQ-ECOF can be attributed to its highly porous skeleton and shortened Li^+ diffusion paths.

The theoretical capacity of DAAQ-ECOF, DABQ-ECOF and TEMPO-ECOF is calculated from the following Eq. (3):

$$C_t = \frac{F}{3600(M_w/1000)} \quad (3)$$

where F and M_w is the Faraday constant (96484 C mol^{-1}) and the molecular weight per active specie, respectively.

The molecular weight of DAAQ-ECOF is 1062 g mol^{-1} , and there are 6 anquinone groups served as active sites in each unit cell. Thus the molecular weight per active specie ($M_w = M_{\text{unit cell}}/6$) is 177 g mol^{-1} , and the theoretical capacity is evaluated as 151 mA h g^{-1} ; The molecular weight of DABQ-ECOF is 728 g mol^{-1} per unit cell, and there are 6 quinone groups served as active sites in each unit cell. Thus the molecular weight per active specie ($M_w = M_{\text{unit cell}}/6$) is 121 g mol^{-1} , and the

theoretical capacity is evaluated as 221 mA h g⁻¹; The molecular weight of TEMPO-ECOF is 2489 g mol⁻¹ per unit cell, and there are 6 nitroxide radical groups served as active sites in each unit cell. Thus the molecular weight per active specie ($M_w = M_{\text{unit cell}}/12$) is 207 g mol⁻¹, and the theoretical capacity is evaluated as 129 mA h g⁻¹.

In order to illustrate the advantages of the present strategy, we fabricated another three kinds of electrodes as the controlled experiments. One is using hand grind method to prepare the electrodes slurry (DAAQ-ECOF-hand), and its cycling capacity is only 80 mA h g⁻¹ at 20 mA g⁻¹. The TEM and AFM images of DAAQ-ECOF-25 Hz indicate its thickness is ranging from 15 to 25 nm (Figure S4), and it delivers a capacity of 120 mA h g⁻¹ at 20 mA g⁻¹ (Figure S5). The capacity of DAAQ-ECOF-60 Hz decreased significantly after ten cycles, resulting from the partially decomposed of the sample at relatively high frequency and long milling time (Figure S5). To sum up, we have adjusted the ball-milling conditions and found that 50 Hz/0.5 h is the optimal conditions to afford exfoliated DAAQ-TFP-COF with better electrochemical performance.

As a highly porous crystalline material, the volumetric capacity of COF might be low comparing to some close-packed oxide anion array. However the volumetric capacity is only one of the important factors for some portable energy applications, like those in electronic devices and EVs. Indeed, many other energy storage solutions need to balance the overall performance in volumetric density, gravimetric density, cost, environmental footprint, long-term stability and high-rate capability. For example, cycle performance and rate capacity are critical for grid-scale applications due to the following reasons: 1) good cycle performance will lead to a low energy storage cost per cycle; 2) excellent rate performance is the prerequisite for grid-scale renewable energy storage since such alternative energy sources are often fluctuating daily and seasonally, it is needed that the energy capacity remains steady at changing charge/discharge rates. Our studies have shown that COFs can serve as promising alternatives for such critical applications. We proposed a novel strategy by designing an extended and stable 2D few-layer polygon sheet rich in quinone moieties (DAAQ-ECOF) to promote reversible charge/discharge capacity and improve cycle performance. At the same time, the active sites anchored to the inner surfaces and

edges of exfoliated COF can be sufficiently exposed and reacted during fast charge/discharge process, and thus ensuring well-performed rate capacity. Moreover, the atomically controllable and highly crystalline features of COFs enable fine tuning of capacity (including both gravimetric capacity and volumetric capacity) and provide a platform for better understanding of diffusion mechanisms and electrochemical process of active sites.

4. Supplementary Figures

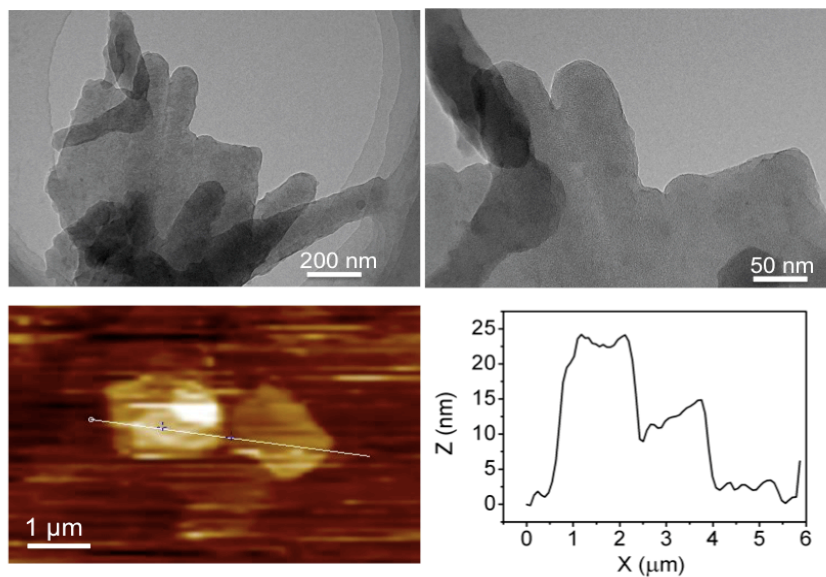


Figure S4. TEM and AFM images along with height profile of DAAQ-ECOF-25Hz.

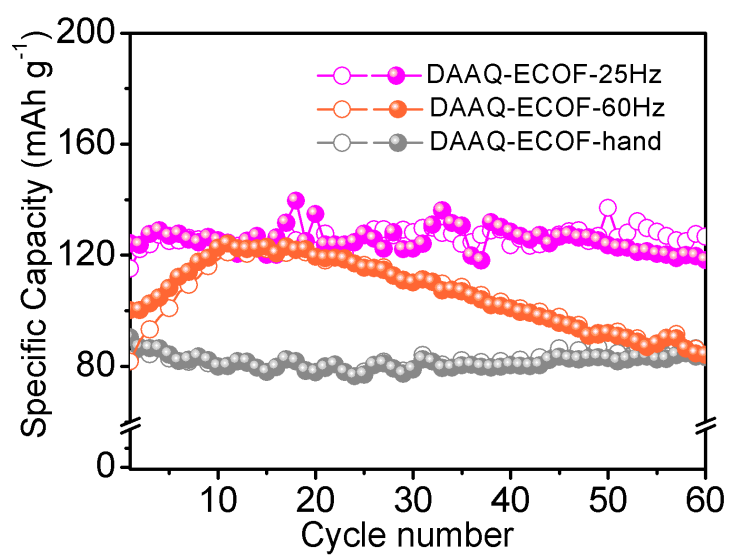


Figure S5. Cycling performance of DAAQ-ECOF-25Hz, DAAQ-ECOF-60Hz and DAAQ-ECOF-hand at a current density of 20 mA g^{-1} .

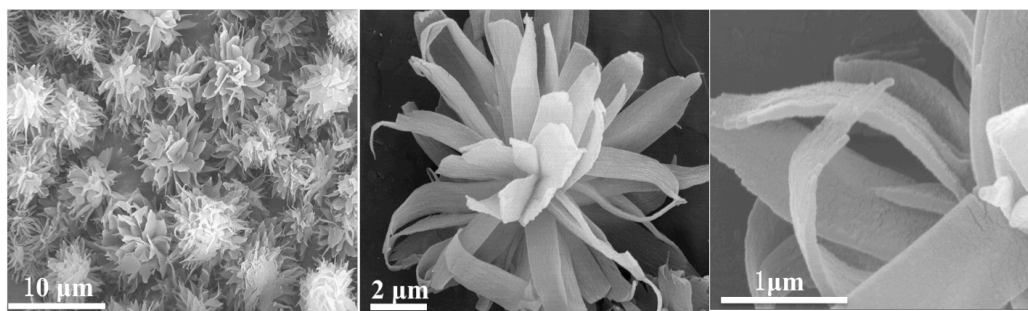


Figure S6. SEM images of DAAQ-TFP-COF.

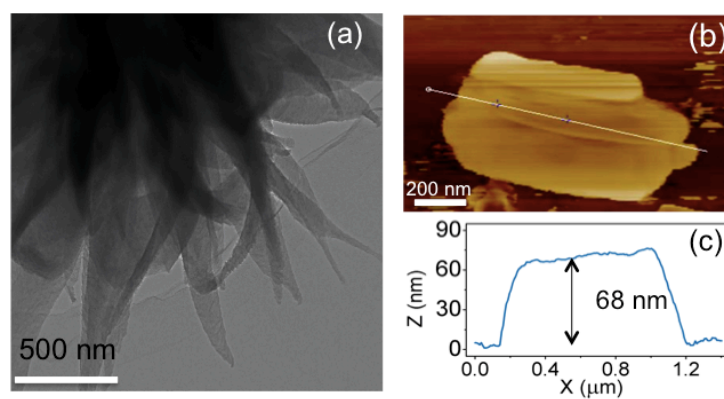


Figure S7. TEM photo, AFM topographical image and height profile of DAAQ-TFP-COF.

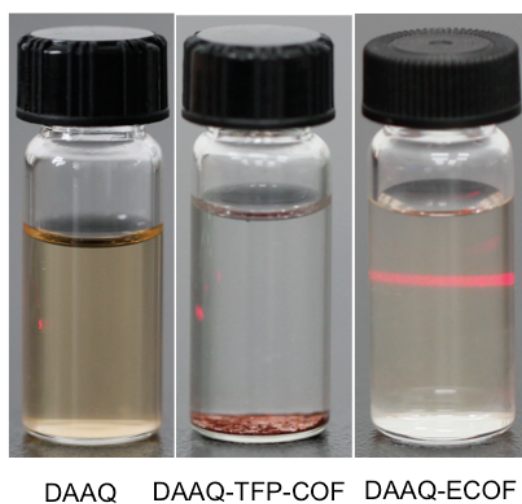


Figure S8. Tyndall tests for the MeOH solutions of DAAQ, DAAQ-TFP-COF and DAAQ-ECOF. Only DAAQ-ECOF solution still exhibited Tyndall effect after 24 h.

Table S1. Elemental analysis results of DAAQ-TFP-COF, DAAQ-ECOF, DABH-TFP-COF, DABQ-TFP-COF, TAPB-BPTA-COF and TEMPO-COF.

COFs		C%	N%	H%
DAAQ-TFP-COF	Anal. Calcd .	70.12	8.13	2.99
	Found.	68.40	8.24	5.13
DAAQ-ECOF	Anal. Calcd .	70.12	8.13	2.99
	Found.	66.49	8.02	4.02
DABH-TFP-COF	Anal. Calcd .	59.02	11.47	3.30
	Found.	56.65	11.13	3.60
DABQ-TFP-COF	Anal. Calcd .	59.35	11.53	2.27
	Found.	57.29	11.47	2.5
TAPB-BPTA-COF	Anal. Calcd .	81.5	6.34	4.87
	Found.	79.5	5.98	4.46
TEMPO-COF	Anal. Calcd .	68.60	16.67	7.12
	Found.	68.13	16.00	6.75

The calculated elemental weight for DAAQ-ECOF is estimated based on the guest-free samples, which are treated as infinite 2D polygon sheets with a chemical formula of $C_{10}H_5O_2N_1$. Experimental result reveals that the C, H, and N contents are close to the calculated values. The slight deviation may result from the edge groups in the polygon sheet with few incomplete structural units or defects in the extended framework. In addition, the consistence of DAAQ-ECOF before and after exfoliation in the EA results indicates that the chemical composition remains intact after mechanical ball-milling treatment.

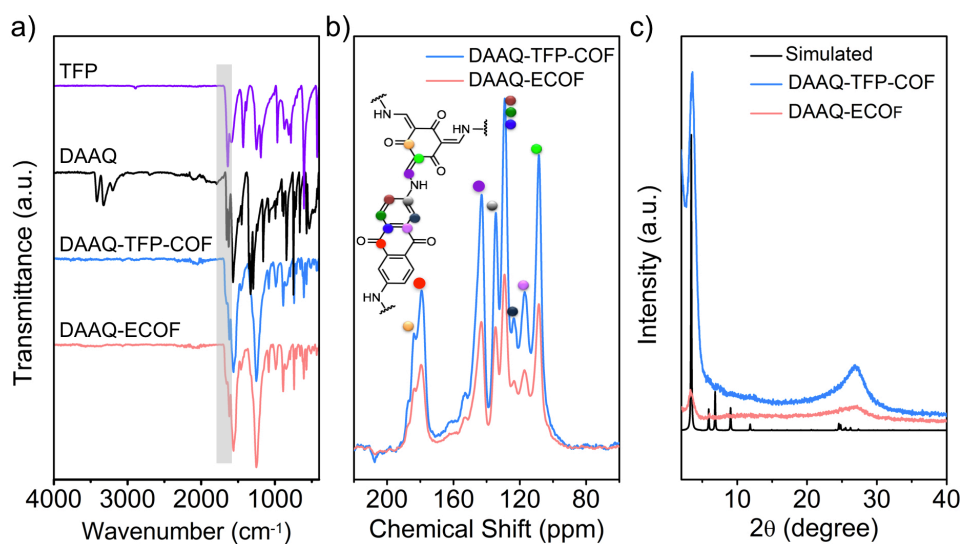


Figure S9. (a) IR spectra of TFP, DAAQ, DAAQ-TFP-COF and DAAQ-ECOF. (b) ^{13}C CP-MAS solid-state NMR spectra and (c) PXRD patterns of DAAQ-TFP-COF and DAAQ-ECOF.

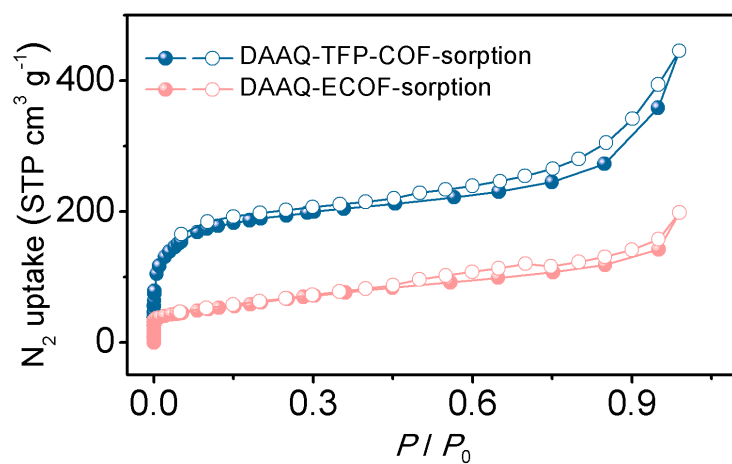


Figure S10. Nitrogen sorption profiles of DAAQ-TFP-COF and DAAQ-ECOF.

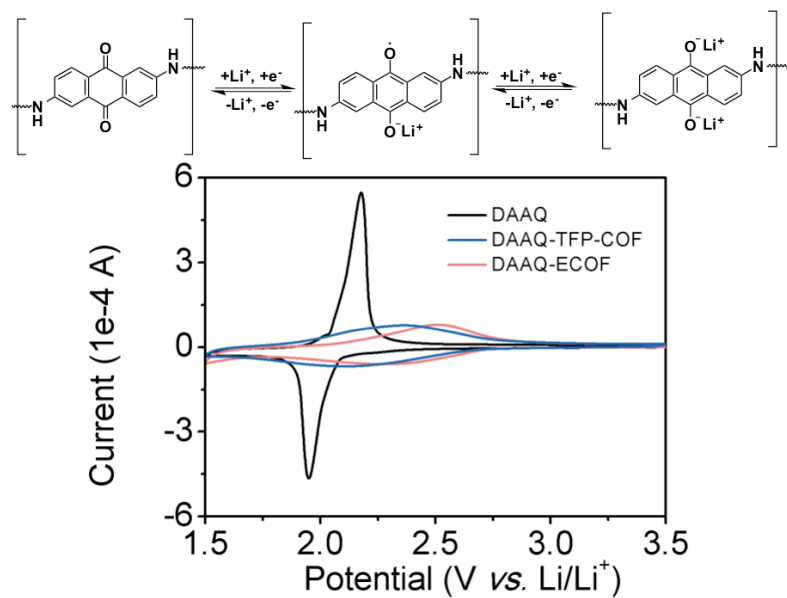


Figure S11. Electrochemical redox reactions of the DAAQ unit and cyclic voltammograms (CVs) of DAAQ, DAAQ-TFP-COF and DAAQ-ECOF at a scan rate of 0.02 mV s⁻¹.

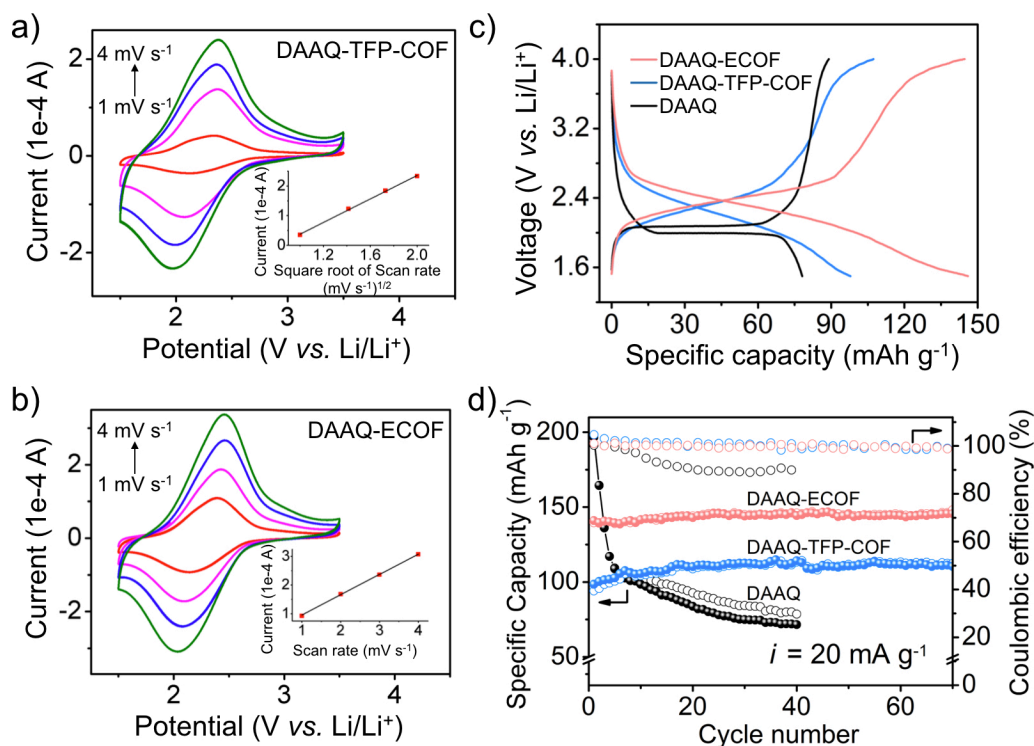


Figure S12. CV curves of (a) DAAQ-TFP-COF and (b) DAAQ-ECOF at different scan rates. The insets show the linear relation of cathodic peak current vs. square root of scan rate ($y = 1.982x - 1.607$, $R^2 = 0.9980$) and cathodic peak current vs. scan rate ($y = 0.7070x + 0.2514$, $R^2 = 0.9975$) for DAAQ-TFP-COF and DAAQ-ECOF, respectively. (c) Discharge–charge curves for the 15th cycle and (d) cycling performance and Coulombic efficiencies of DAAQ, DAAQ-TFP-COF and DAAQ-ECOF at a current density 20 mA g^{-1} . The electrode was pre-activated 2 cycles at 10 mA g^{-1} before starting the measurements.

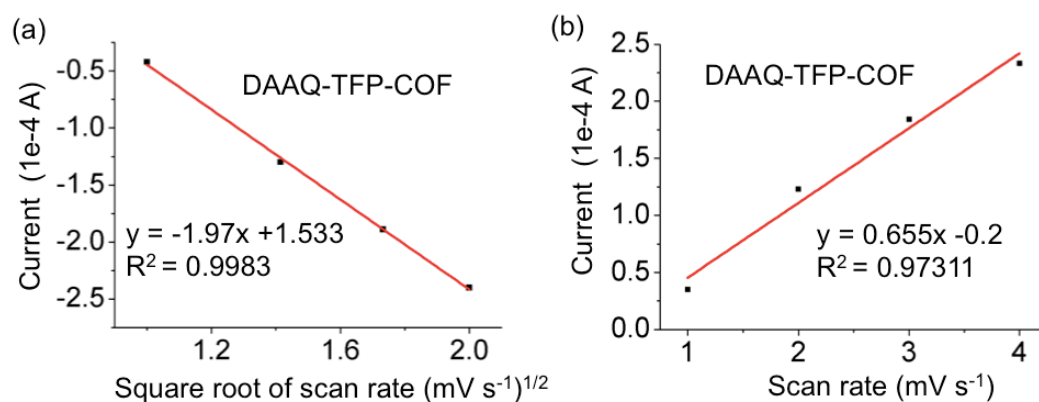


Figure S13. (a) The linear relation of anodic peak current vs. square root of scan rate of DAAQ-TFP-COF. (b) The linear fit of cathodic peak current vs. scan rate of DAAQ-TFP-COF.

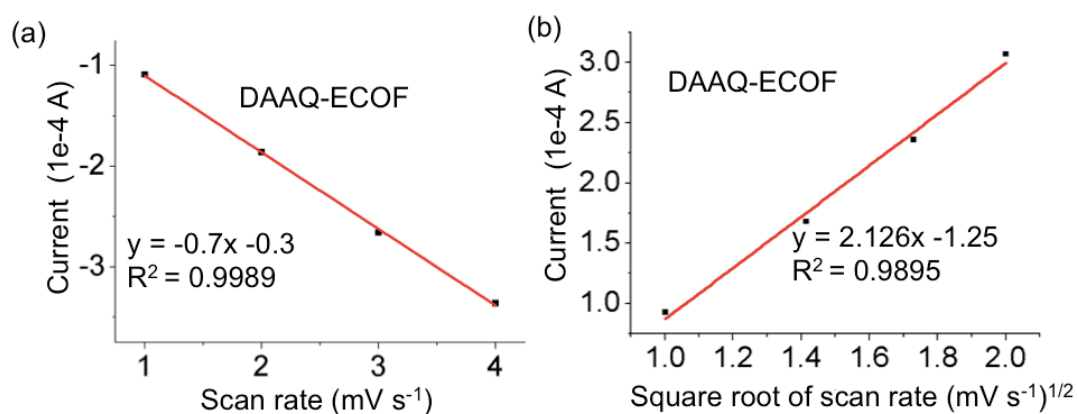


Figure S14. (a) The linear relation of anodic peak current vs. scan rate of DAAQ-ECOF. (b) The linear fit of cathodic peak current vs. square root of scan rate DAAQ-ECOF.

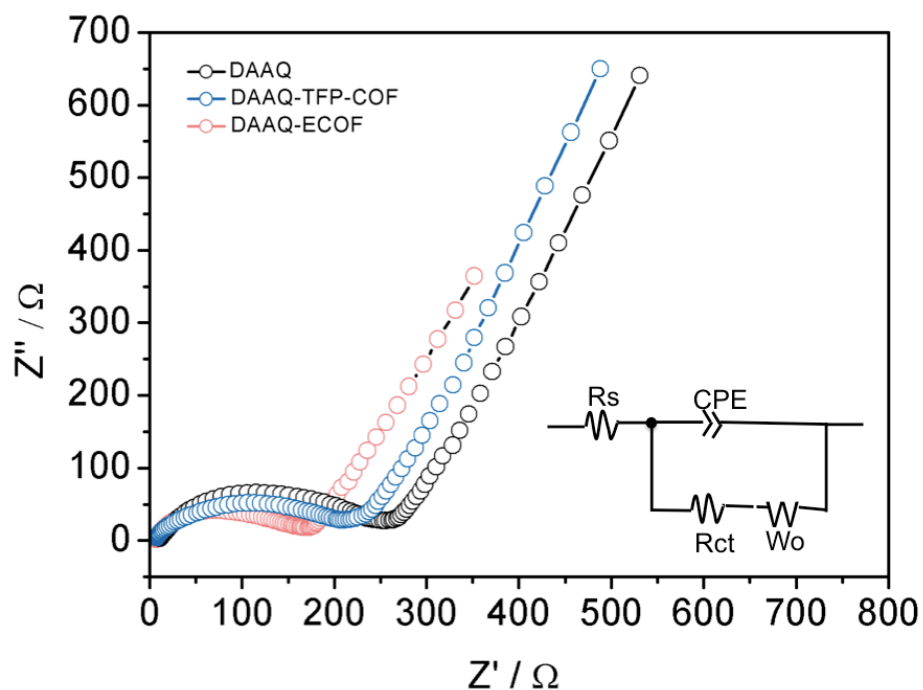


Figure S15. EIS of DAAQ, DAAQ-TFP-COF and DAAQ-ECOF electrodes. The inset shows the equivalent circuit used for fitting the electrochemical impedance data. The R_s , R_{ct} , CPE and W represent solution resistance, charge-transfer resistance, constant phase element and Warburg impedance, respectively.

Table S2. Fitted values of elements in the equivalent circuit for EIS data of DAAQ, DAAQ-TFP-COF and DAAQ-ECOF electrodes.

	R_s (Ω)	CPE1-T	CPE1-P	R_{ct} (Ω)	Wo-R	Wo-T	Wo-P
DAAQ	8.922	3.46×10^{-5}	0.675	236.9	150.3	2.096	0.374
DAAQ-TFP-COF	6.074	2.64×10^{-5}	0.716	198.7	233	2.437	0.375
DAAQ-ECOF	5.828	3.26×10^{-5}	0.713	148.5	25.59	0.299	0.348

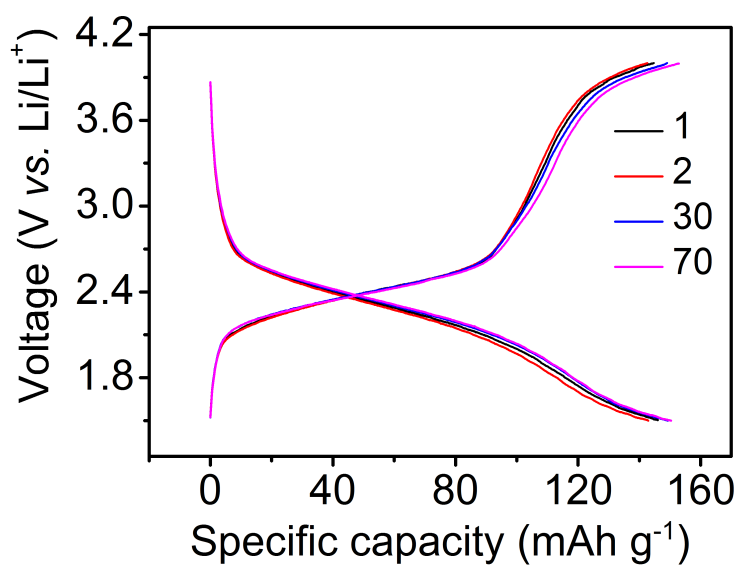


Figure S16. Discharge–charge curves of DAAQ-ECOF (1st, 2nd, 30th, and 70th cycles are selected as representatives).

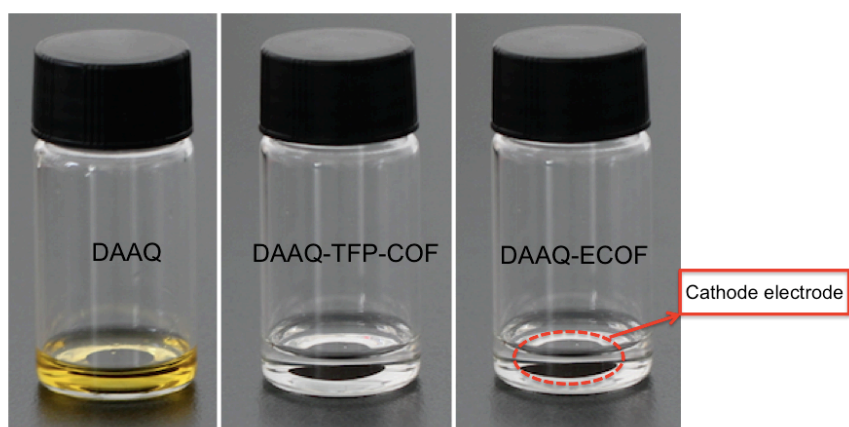


Figure S17. Solubility tests for DAAQ, DQQA-TFP-COF and DAAQ-ECOF electrodes. In each vial, the electrode was immersed in 1 mL of the electrolyte (1 M LiTFSI/TEGDME) for 48 h.

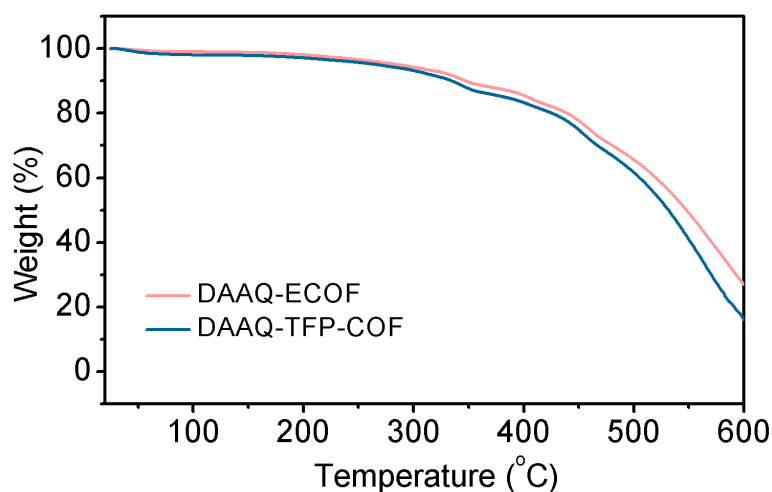


Figure S18. TGA profiles of DAAQ-ECOF and DAAQ-TFP-COF after activation.

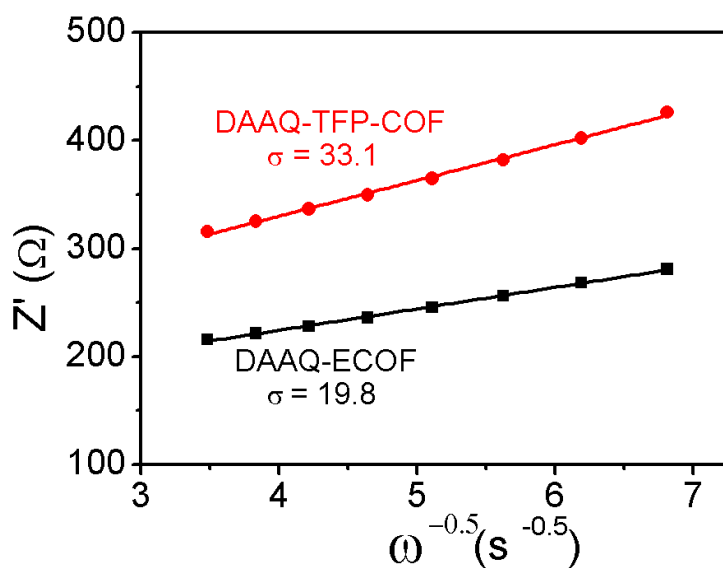


Figure S19. The plot of Z_{re} vs. the inverse square root of angular frequency (ω) for the he DAAQ-TFP-COF and DAAQ-ECOF batteries. The slopes of the fitted lines represent the Warburg coefficient σ .

Table S3. Lithium ion diffusion coefficients (D_{Li^+}) of DAAQ-TFP-COF, DAAQ-ECOF and some commercial inorganic electrodes.

	D_{Li^+} ($\text{cm}^2 \text{s}^{-1}$)	Reference
DAAQ-ECOF	6.94×10^{-11}	This work
DAAQ-TFP-COF	2.48×10^{-11}	This work
LiFePO_4	5.2×10^{-14}	Ref [9]
LiMnO_2	3.4×10^{-12}	Ref [11]
$\text{Li}(\text{Ni}_{0.5}\text{Mn}_{0.3}\text{Co}_{0.2})$	1.7×10^{-11}	Ref [12]
$\text{LiNi}_{0.5}\text{Mn}_{0.5}\text{O}_2$	1.41×10^{-13}	Ref [13]

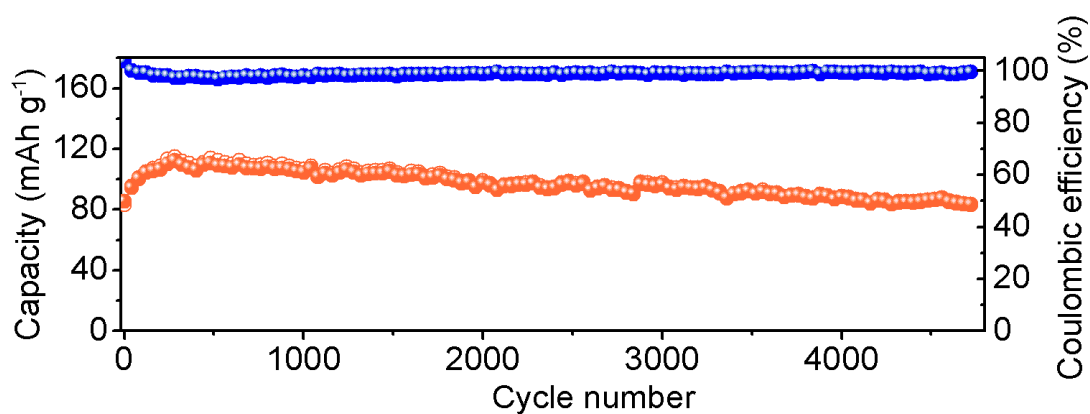


Figure S20. Long-term cycling performance of DAAQ-ECOF at a current density of 500 mA g^{-1} . The capacity remains above 85 mA h g^{-1} after 4750 cycles, further demonstrating the excellent cycling stability of our material. Indeed this performance is already superior comparing to many commercial cathode materials (LiCoO_2 or $\text{LiNi}_{0.6}\text{Co}_{0.2}\text{Mn}_{0.2}$)^[14-15].

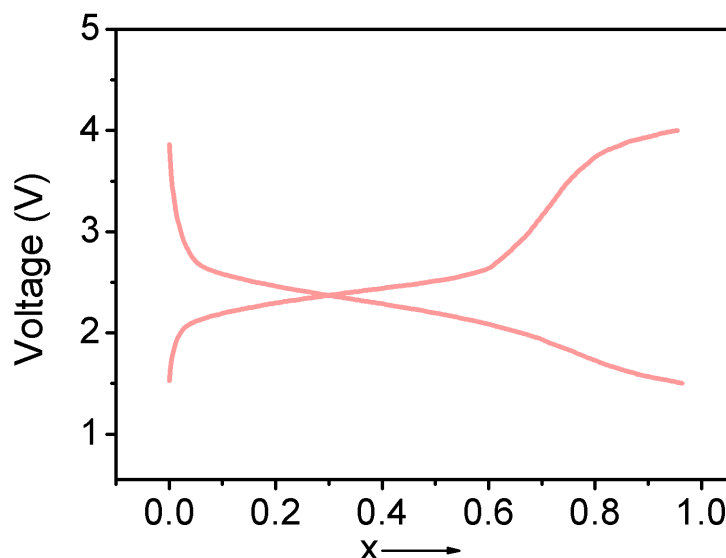


Figure S21. Voltage profile for a $\text{Li}/\text{C}_{10}\text{H}_5\text{O}_2\text{N}_1$ DAAQ-ECOF half cell cycled between 1.5 and 4 V at 20 mA g^{-1} (x is the value in $[\text{Li}_x\text{C}_{10}\text{H}_5\text{O}_2\text{N}_1]$).

We have calculated the movement of Li ion during charge and discharge process according to the following Eq. (4):

$$\text{Capacity} = \frac{x \times F}{3600(M_w/1000)} \quad (4)$$

where F is the Faraday constant (96484 C mol^{-1}), M_w is the molecular weight per active specie (one quinone group) in DAAQ-ECOFs ($\text{Li}_x\text{C}_{10}\text{H}_5\text{O}_2\text{N}_1$), x is the value of transport Li ion number during charge/discharge process.

As shown in the Figure S21, during discharge, the movement number of Li ion is 0.05 at 2.5 V, then the platform appears until $x = 0.7$ at 2.2 V, and finally reaches 0.97 at 1.5 V; after recharge process, all of the Li ions can be sufficiently removed. These results indicate that the DAAQ-ECOF exhibits good reversible capacity during charge/discharge processes.

The intense PXRD diffraction peaks of DABQ-TFP-COF and TEMPO-COF indicates that the building units are arranged periodically in these two COFs. For DABQ-TFP-COF, the peak at 4.46° reveals regularly aligned pores with a d_{100} spacing of 22.809 \AA in the XY plane, while the (001) facet at 26.25° originates from stacking with a d_{001} inter-sheet interval of 3.4 \AA along the Z direction. For TEMPO-COF, the diffraction peaks at 2.78 and 4.80 are attributed to the (100) and (110) facets, respectively. Pawley refinement confirmed the diffraction assignments

and gave a good match to the observed XRD patterns for both two COFs, as evidenced by negligible differences (Figure S22, black and blue curves). Crystalline structure simulations using the Reflex Plus module of the Materials Studio programs produced unit-cell parameters of $\alpha = \beta = 90^\circ$, and $\gamma = 120^\circ$, $a = b = 22.792 \text{ \AA}$, and $c = 3.4 \text{ \AA}$ for DABQ-TFP-COF and $\alpha = \beta = 90^\circ$, and $\gamma = 120^\circ$, $a = b = 37.603 \text{ \AA}$, and $c = 3.4 \text{ \AA}$ for TEMPO-COF. The packing structures were built using AA stacking models of the *P3* space group, where atoms in adjacent sheets lie on top of each other, and an AB stacking models of the *P1* space group, where the sheets are offset by 1/2, 1/2 (Figure S22). The simulated XRD patterns of the AA stacking model matched the experimental peak positions and intensities quite well (Figure S22, green curve). In contrast, the staggered AB stacking arrangement did not match with the experimental data (Figure S22, pink curve).

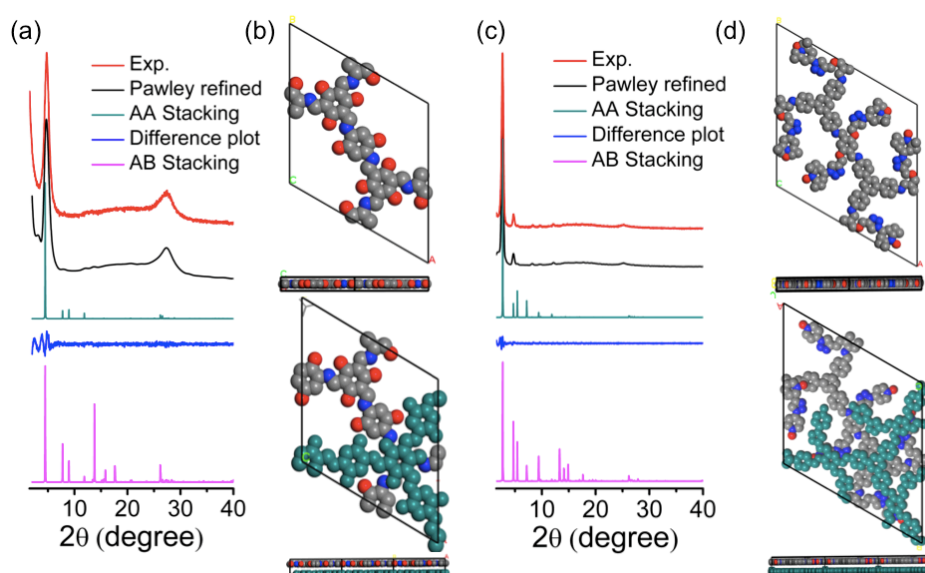


Figure S22. (a and c) PXRD pattern simulations of DABQ-TFP-COF and TEMPO-COF. The red curves are experimentally observed XRD patterns, black curves are Pawley refinements and blue curves are their difference; the green curve are the simulated XRD patterns based on the AA stacking models and pink curves are that based on the AB stacking models. (b and d) The unit-cell structures of DABQ-TFP-COF and TEMPO-COF derived using the AA and AB stacking models.

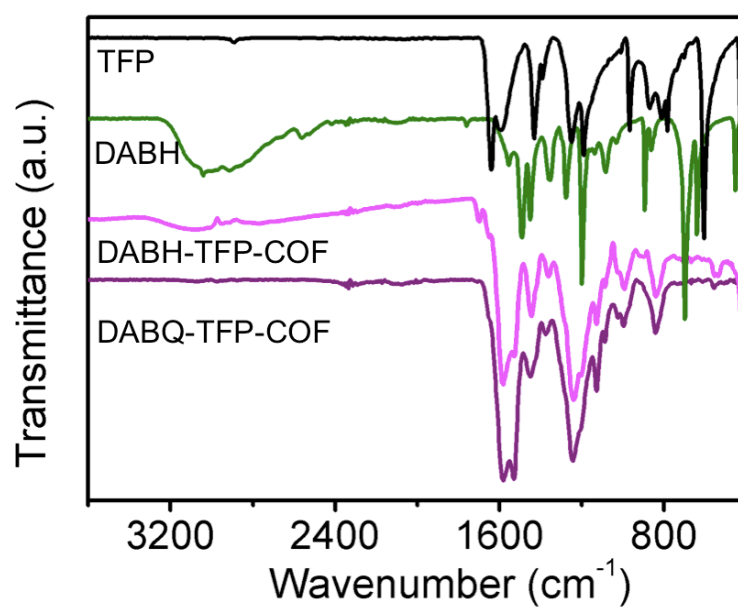


Figure S23. IR spectra of TFP, DABH, DABH-TFP-COF and DABQ-TFP-COF.

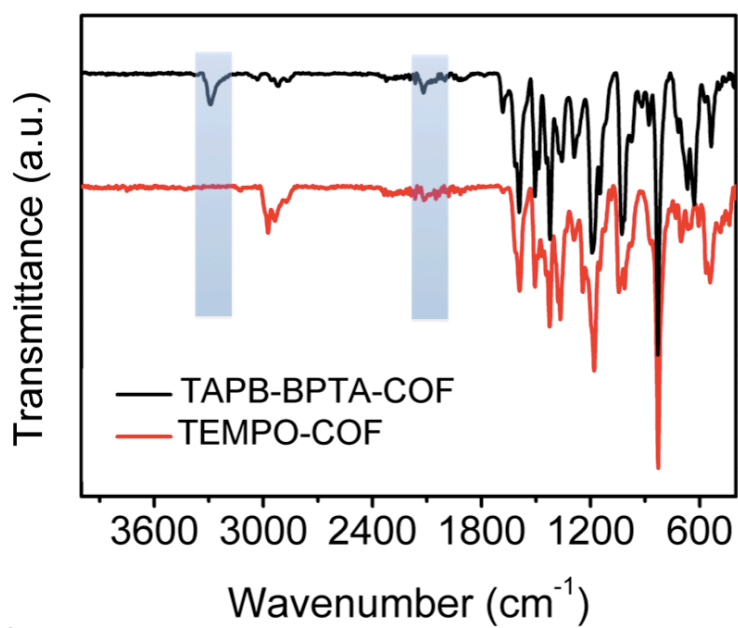


Figure S24. IR Spectra of TAPB-BPTA-COF and TEMPO-COF.

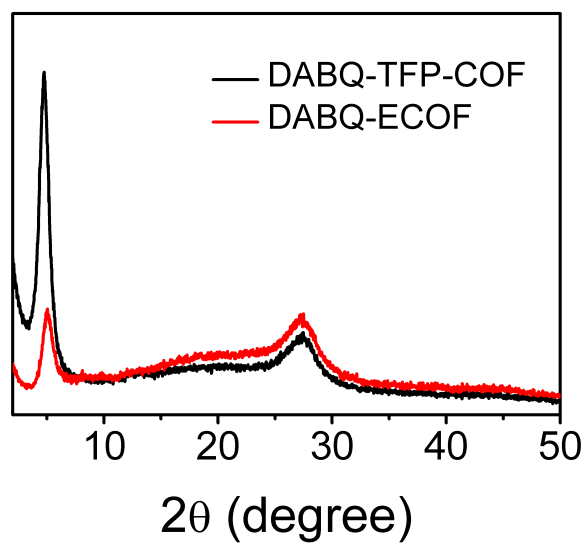


Figure S25. PXRD patterns of DABQ-TFP-COF and DABQ-ECOF.

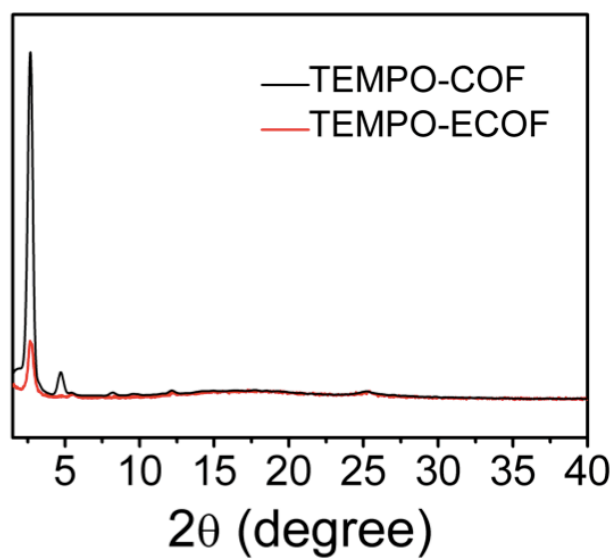


Figure S26. PXRD patterns of TEMPO-COF and TEMPO-ECOF.

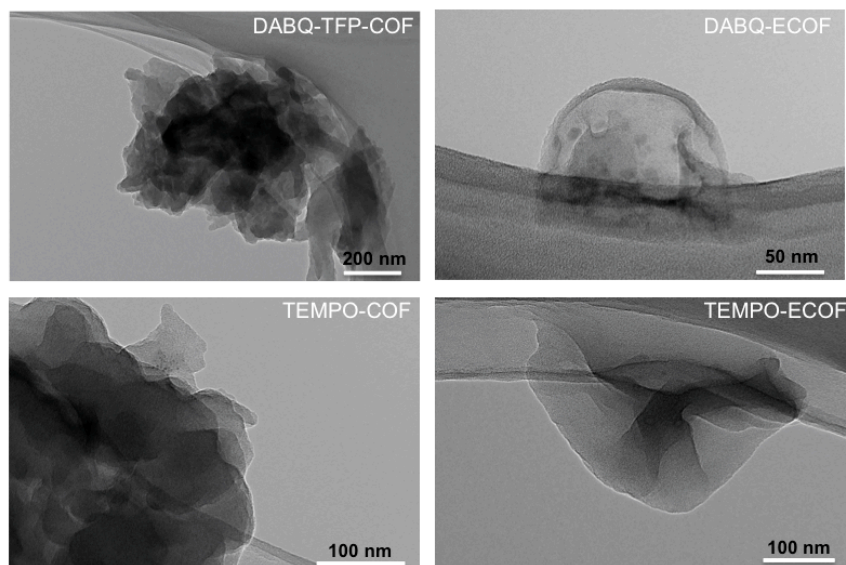


Figure S27. TEM photos of DABQ-TFP-COF, DABQ-ECOF, TEMPO-COF and TEMPO-ECOF.

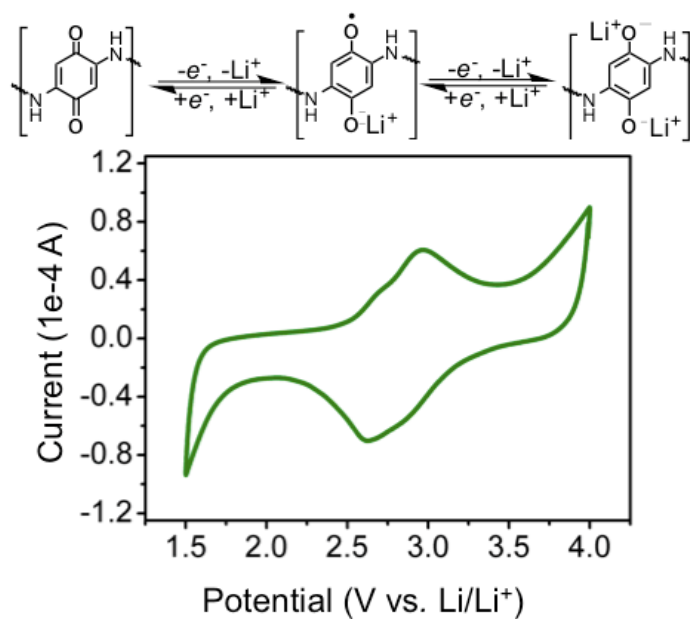


Figure S28. Electrochemical redox reactions of the DABQ unit and cyclic voltammograms of DABQ-ECOF at scan rate of 0.01 mV s⁻¹.

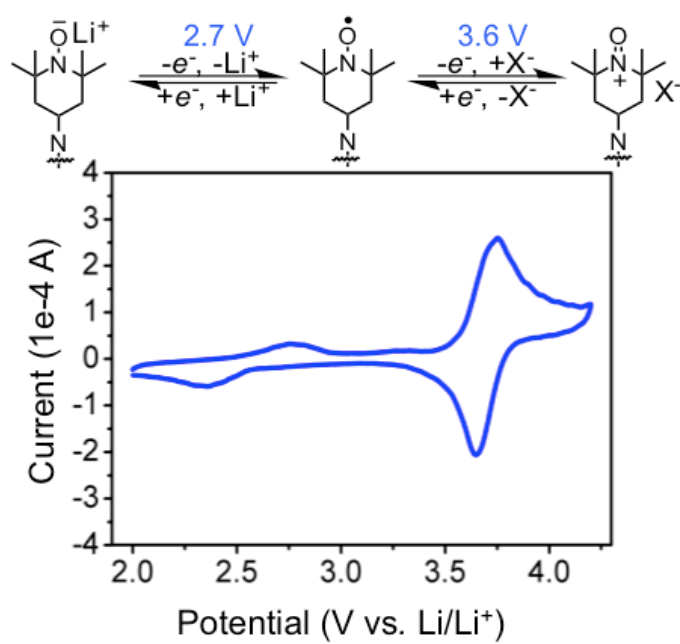
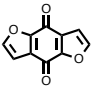
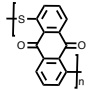
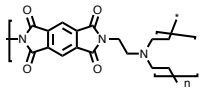
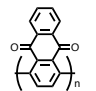


Figure S29. Electrochemical redox reactions of the TEMPO unit and cyclic voltammograms of the TEMPO-ECOF at scan rate of 0.01 mV s⁻¹.

Table S4. Comparison of cathode materials in Lithium-ion battery.

Materials	Discharge Voltage (V)	Discharge Capacity (mA h g ⁻¹)	Current	Cycling number	Capacity retention	Ref.
LiFePO ₄	3.4	140	0.1 C	10	100%	<i>Adv. Mater.</i> 2007 , <i>19</i> , 1963.
LiMn ₂ O ₄	3.8	120	0.5 C	3	90%	<i>Nano Lett.</i> 2014 , <i>14</i> , 993
LiCoO ₂	3.7	155	0.28 C	100	65%	<i>Chem. Commun.</i> 2015 , <i>51</i> , 12391
LiNi _{0.8} Co _{0.1} Mn _{0.1} O ₂	3.6	217.4	0.2 C	100	55.5%	<i>ACS Appl. Mater. Interfaces</i> 2015 , <i>7</i> , 7702.
	2.6 and 2.27	233	0.1C	5	86%	<i>Adv. Energy Mater.</i> 2013 , <i>3</i> , 600
	2.2	170	0.1 C	100	95%	<i>Nano Lett.</i> 2012 , <i>12</i> , 2205.
	2.21	179	0.5 C	200	86.6%	<i>Adv. Mater.</i> , 2015 , <i>27</i> , 6504
	2.14	263	0.2 C	10	100%	<i>Angew. Chem. Int. Ed.</i> 2015 , <i>54</i> , 13947.
DAAQ-ECOF	2.3	145/107	0.13 C /3.25C	80/1800	100% /98%	This work
DABQ-ECOF	2.8	210	0.1 C	20	97%	This work
TEMPO-ECOF	3.6 and 2.7	115	0.16 C	3	90%	This work

References

- [1] Chong, J. H.; Sauer, M.; Patrick, B. O.; MacLachlan, M. J. *Org. Lett.* **2003**, *5*, 3823.
- [2] DeBlase, C. R.; Silberstein, K. E.; Truong, T. T.; Abruna, H. D.; Dichtel, W. R. *J. Am. Chem. Soc.* **2013**, *135*, 16821.
- [3] Okada, Y.; Sugai, M.; Chiba, K. *J. Org. Chem.* **2016**, *81*, 10922;
- [4] Lingam, V. S. P. R.; Vinodkumar, R.; Mukkanti, K.; Thomas, A. ; Gopalan, B. *Tetrahedron Lett.* **2008**, *49*, 4260.
- [5] Tansakul, C.; Lilie, E.; Walter, E. D.; Rivera, F.; Wolcott, A.; Zhang, Z. J.; Millhauser, G. L.; Braslau, R. *J. Phys. Chem. C* **2010**, *114*, 7793.
- [6] Wu, H.; Meng, Y.; Lu, K.; Wei, Z. *J. Mater. Chem. A* **2013**, *1*, 6366.
- [7] Wang, G. X.; Yang, L.; Chen, Y.; Wang, J. Z.; Bewlay, S.; Liu, H. K. *Electrochim. Acta* **2005**, *50*, 4649.
- [8] Ho, C.; Raistrick, I. D.; Huggins, R. A. *J. Electrochem. Soc.* **1980**, *127*, 343.
- [9] Cui, Y.; Zhao, X.; Guo, R. *Electrochim. Acta* **2010**, *55*, 922.
- [10] Ma, Z.; Peng, Y.; Wang, G.; Fan, Y.; Song, J.; Liu, T.; Qin, X.; Shao, G. *Electrochim. Acta* **2015**, *156*, 77.
- [11] Tang, S. B.; Lai, M.O.; Lu, L. *Mater. Chem. Phys.* **2008**, *111*, 149.
- [12] Yang, S.; Wang, X.; Yang, X.; Bai, Y.; Liu, Z.; Shu, H.; Wei, Q. *Electrochim. Acta* **2012**, *66*, 88.
- [13] Wang, X.; Hao, H.; Liu, J.; Huang, T.; Yu, A. *Electrochim. Acta* **2011**, *56*, 4065.
- [14] Qi, P.; Han, Y.; Zhou, J.; Fu, X.; Li, S.; Zhao, J.; Wang, L.; Fan, X.; Feng, X.; Wang, B. *Chem. Commun.* **2015**, *51*, 12391.
- [15] Li, S.; Fu, X.; Zhou, J.; Han, Y.; Qi, P.; Gao, X.; Feng, X.; Wang, B. *J. Mater. Chem. A* **2016**, *4*, 5823.